Surcace roughness classification for castings

D. M. Tsai and C. F. Tseng
Machine Vision Lab.
Department of Industrial Engineering and Management
Yuan-Ze University, Chung-Li, Taiwan, R.O.C.
E-mail: iedmtsai@saturn.yzu.edu.tw

1. INTRODUCTION

The proper functioning of a machined part is in many instances largely dependent on the quality of its surface. Engineering properties such as fatigue, hardness and heat transfer are affected by surface finish. Several devices have been developed to measure surface roughness (Amstead et al. 1987). The simplest procedure is a visual comparison with an established standard, while the most commonly used method is to employ a diamond stylus to trace over the surface being investigated and to record a magnified profile of the irregularities. These are generally time-consuming processes, demanding expensive human intelligence.

In this study, we investigate the measurement of surface roughness of shaped and milled parts using machine vision. Machine vision allows the assessment of surface roughness without touching or scratching, which are two problems with traditional methods. It provides the advantages of a measurement process for 100% inspection and the flexibility for measuring the part under test without fixing it in a precise position. In contrast to the stylus-based methods that trace the surface roughness in one dimension, machine vision can

generate many more readings of a two dimensional surface in a given time and, therefore, makes the estimation method for roughness measurement more reliable.

Over the years, the non-contact optical methods have attracted researchers' attention for the assessment of surface roughness. Most of the methods are based on statistical measures of gray-level images in the spatial domain. Al-Kindi et al. (1992) examined the use of a digital image system in the assessment of surface quality. The measure of surface roughness is based on spacing between gray-level peaks and number of gray-level peaks per unit length of a scanned line in the gray-level image. This 1-D based technique does not fully utilize the 2-D information of the surface image, and is sensitive to lighting and noise. Luk and Huynh (1987) utilized the gray-level histogram (distribution) of the surface image to characterize surface roughness. They found the ratio of the spread and the mean value of the distribution is a nonlinear, increasing function of average surface roughness R_a (center line average). Since their method is based soley on gray-level histogram, it is sensitive to the uniformity and degree of illumination present. In addition, no information regarding the spatial distribution of periodic features can be obtained from the gray-level histogram. Hoy and Yu (1991) adopted the algorithm of Luk and Huynh to characterize surface quality of turned and milled specimens. In their experiments, they found one exception that the ratio of the spread and the mean of the gray-level distribution is not a monotonically increasing function of surface roughness and, therefore, the value of the ratio may lead to incorrect measurement. Hoy and Yu also addressed the possibility of using the Fourier transform (FT) to characterize surface roughness in the frequency domain. However, only simple visual judgement of surface images in the frequency plane is discussed. No quantitative description

of FT features for the measurement of surface roughness is proposed. Other non-contact optical proximity methods, which include lasers and fiber optics (Scott and Baul 1980) and complicated Moire interferometric technigue (Chen et al. 1994) available for surface roughness measurement are hardware limited and require high eguipment cost.

In this study, we use machine vision to estimate the surface roughness of machined parts generated by shaping and milling processes. The quantitative measures of surface roughness are extracted in the spatial frequency domain using the two-dimensional Fourier transform. The Fourier transform approach has the desirable properties of noise-immunity, orientational dependency, and enhancement of periodic features. A FT pattern feature is proposed to distinguish between shaped and milled surfaces in a given range of surface roughness. A set of five roughness features extracted from the frequence plane is presented as the measures of surface roughness for both shaped and milled surfaces.

Artificial neural networks (*ANNs*), which take roughness features as the input, are applied to classify the surface of interest among a set of standard surfaces of known roughness values. Two neural network models are developed. The first network is for workpieces in a fixed orientation, which minimizes the deviation of roughness measures. Only the roughness features are used as the input to the network. The second network is for workpieces in arbitrary orientations, which gives maximum flexibility for inspection tasks. The roughness features along with the surface direction derived from the FT frequency plane are used as the input to the network. By using these tow *ANNs* with roughness features extracted from the frequency plane, accurate and flexible automated visual measurement of

surface roughness can be achieved.

This paper is organized as follows: Section 2 discusses the extraction of surface roughness features in the spatial frequency domain. Section 3 presents the neural network models for estimating surface roughness. A feature selection procedure that chooses the best subset of features as the input to the network is also addressed in this section. Section 4 presents the experimental results for two sets of shaped and milled specimens with various roughness standards. The paper is conclude in Section 5.

2. EXTRACTION OF ROUGHNESS FEATURES

The first and most important task in roughness measurement with machine vision is to extract roughness features of surfaces. Typical noise processes tend to dramatically alter local spatial variation of intensity while having relatively uniform representation in spatial frequency (Liu and Jernigan 1990). Frequence domain features should be less sensitive to noise than spatial domain features. Therefore, in this study we choose to extract features of surface roughness in the spatial frequency domain using the 2-D Fourier transform. The FT is particularly useful for surfaces in noisy conditions due to tool wear marks, dust and dirt. The FT characterizes the surface image in terms of frequency components. The periodically-occurring features such as feedmarks and toolmarks present in the gray-level image can be easily observed from the magnitude of the frequency components. Furthermore, the FT is rotation- dependent, i.e., rotating the original image by an angle will rotate its corresponding frequency plane by the same angle. The lay direction of a surface

can be preserved accordingly.

Let $f(x, y)$ be the gray level of a pixel at (x, y) in the original image of size $N \times N$ pixels centered on the origin. The discrete 2-D Fourier transform of $f(x, y)$ is given by

$$F(u,v) = \frac{1}{N} \sum_{x=-\frac{N}{2}}^{\frac{N}{2}-1} \sum_{y=-\frac{N}{2}}^{\frac{N}{2}-1} f(x, y) \cdot exp\left[-j2p(ux+vy)/N\right] \qquad (1)$$

for $u, v = -\frac{N}{2}, -\frac{N}{2}+1,\ldots,0, 1,\ldots, \frac{N}{2}-1$. The discrete 2-D Fourier transform can be expressed in the separatable forms with 1-D Fourier transforms, and obtained efficiently using the fast Fourier transform algorithm (Gonzalez and Woods 1992).

The Fourier transform is generally complex; that is

$$F(u,v) = R(u,v) + j \cdot I(u,v)$$

where $R(u,v)$ and $I(u,v)$ are the real and imaginary components of $F(u,v)$, respectively. The power spectrum $P(u,v)$ of $f(x, y)$ is defined by

$$P(u,v) = |F(u,v)|^2 = R^2(u,v) + I^2(u,v)$$

In this study we have focused on roughness measurements of shaped and milled surfaces. Figures 1(a), 1(b) and 1(c) show the surface images of three shaped specimens with the roughness values of R_{max} 6.3, 25 and 100 mm, respectively, where R_{max} is the distance between the highest peak and the lowest valley in the trace of the surface. Figures 1(d), 1(e) and 1(f) visually show the power spectra $P(u,v)$ of the surface images as an intensity function, where brightness is proportional to the magnitude of $P(u,v)$. Figures 1(g),1(h)

and 1(i) present the plots of the power spectrum functions in 3-D perspective. It can be seen from Figures 1(d) through 1(i) that the origin in the center of the power spectrum map has the largest magnitude of $P(u, v)$. Note that a series of approximately equally-spaced spots of decreasing magnitude of power spectrum are deployed along the horizontal line on both sides of the origin. The distance between adjacent bright spots represents the frequency of the periodic feedmarks in the surface image. The finer the surface roughness, the larger the distance(i.e., the higher the frequency) is resulted. We can also observe that the line passing through these equally-spaced bright spots in the power spectrum map is perpendicular to the direction of lay in the original surface image.

A similar observation can also be made for the milled specimens with three roughness values of R_{max} 1.6, 12.5 and 50 mm as shown in Figures 2(a), 2(b) and 2(c), respectively. By comparing Figures 1(a)-1(c) and Figures 2(a)-2(c), we found that the surface patterns of the shaped specimens are more regular and present less noise than those of the milled specimens. Therefore, multiple diffuse points around the origin in the power spectrum map (Figures 2(d)-2(i)) are generated for milled specimens. These multiple diffuse points correspond to nonperiodic features in the original image.

There may exist a large set of features that can be extracted from the surface image in the frequency domain. However, it is logical to select only such features that their quantitative values are a monotonic function (either increasing or decreasing) with respect to roughness values. This ensures the easy construction of robust estimators for roughness measurement. A set of 28 features (Liu and Jernigan 1990) derived in the frequency domain,

6

which were used for classifying natural textures rather than surface roughness in the field of texture analysis, have been investigated in our preliminary experiments. It has been found that most of the 28 features are not monotonic functions of surface roughness. In this study, we propose five roughness features which are generally (or, approximately) monotonic functions of surface roughness R_{max}. The quantitative definitions of these features are given below. Let

$$p(u,v) = \frac{P(u,v)}{\sum_{(u,v) \neq (0,0)} P(u,v)}$$

be the normalized power spectrum, which has the characteristics of a probability distribution.

1. Major peak frequency F_1

$$F_1 = (u_1^2 + v_1^2)^{1/2}$$

where (u_1, v_1) are the frequency coordinates of the maximum peak of the power spectrum, i.e.,

$$p(u_1, v_1) = max\{ p(u,v), \forall(u,v) \neq (0,0)\}$$

Feature F_1 is the distance of the major peak (u_1, v_1) from the origin $(0,0)$ in the frequency plane. The plots of F_1 values against roughness values R_{max} for both shaped specimens with R_{max} values of 6.3, 12.5, 25, 50 and 100 mm, and milled specimens with R_{max} values of 1.6, 3.2, 6.3, 12.5, 25 and 50 mm are shown in Figure 3. It demonstrates that the value of F_1 decreases as the surface roughness R_{max} increases for both shaped and milled surfaces.

2. Principal component magnitude squared F_2

$$F_2 = l_1$$

where l_1 is the maximum eigenvalue of the covariance matrix of $p(u,v)$. The covariance

matrix M is given by

$$M = \begin{bmatrix} Var(u^2) & Var(uv) \\ Var(vu) & Var(v^2) \end{bmatrix}$$

for which $Var(u^2) = \sum_{(u,v) \neq (0,0)} u^2 \cdot p(u,v)$

$$Var(v^2) = \sum_{(u,v) \neq (0,0)} v^2 \cdot p(u,v)$$

$$Var(uv) = Var(vu) = \sum_{(u,v) \neq (0,0)} uv \cdot p(u,v)$$

Feature F_2 indicates the variance of components along the principal axis in the frequency

plane. From Figure 4, it can be seen that the value of F_2 decreases as the surface

roughness R_{max} increases.

3. Average power spectrum F_3

$$F_3 = \sum_{(u,v) \neq (0,0)} P(u,v) / S$$

where $S = N^2 - 1$ for a surface image of size $N \times N$. Feature 3 is an increasing

function with respect to the surface roughness R_{max} as seen in figure 5.

4. Central power spectrum percentage F_4

$$F_4 = \frac{P(0,0)}{\sum_u \sum_v P(u,v)} \cdot 100\%$$

Based on eq.(1), the frequency component at the origin (the center) of the frequency plane

has the maximum power spectrum. It can be seen from Figure 6 that the value of F_4

decreases as the surface roughness R_{max} increases for both shaped and milled specimens.

5. Ratio of major axis to minor axis F_5

$$F_5 = \left(l_1 / l_2 \right)^{1/2}$$

where l_1 and l_2 are the maximum and minimum eigenvalues of the covariance matrix of

$p(u, v)$. Figure 7 shows the plots of feature F_5 against the roughness R_{max} for both

shaped and milled specimens. Although feature F_5 is not a strictly monotonic function of

roughness R_{max}, it generally agrees with the monotonic tendency when the value of R_{max}

gets larger.

As mentioned previously, the directionality of the frequency components in the

frequency plane indicates the lay direction of a surface in the spatial plane. This phenomenon

can be further observed in Figure 8, where a shaped specimen with roughness R_{max} of

25 $\mathit{m}m$ is rotated by an angle 30°. Note that rotating the original surface image by an angle

30° (Figure 8(a) versus Figure 1(b)) rotates its corresponding frequency plane by the same

angle. The eigenvector associated with eigenvalue l_1 for the covariance matrix of $p(u, v)$

indicates the direction of the principal axis in the frequency plane, and can be basically used

to estimate the direction of a surface. However, a preliminary experiment has shown that the

estimation error of   the eigenvector approach is within 5°. To further improve the

estimation accuracy of direction, we purpose a now direction measure q in this study.

From Figures 1(d)-1(f), 2(d)-2(f) and 8(b), we found that the line passing through a series

of equally-spaced bright spots also passes the origin $(0,0)$ in the frequency plane. Since the distribution of frequency components is symmetric to the central component at $(0,0)$, we can estimate the slope angle q of the best fitting line, in the least sguares sense, by

$$q = tan^{-1} \left[\frac{S_n(uv)}{S_n(u^2)} \right]$$

where $S_n(uv) = \sum_{i=1}^{n} (u_i \cdot v_i) \cdot w(u_i, v_i)$

$$S_n(u^2) = \sum_{i=1}^{n} (u_i)^2 \cdot w(u_i, v_i)$$

$$w(u_i, v_i) = \frac{p(u_i, v_i)}{\sum_{j=1}^{n} p(u_i, v_j)}$$

n is the total number of sample points used for line fitting, which corresponds to the n largest peaks in $p(u, v)$, i.e.,

$$p(u_i, v_i) > p(u_{i+1}, v_{i+1}), \quad p(u_i, v_i) \in \{p(u,v)\}, \quad for \quad i = 1,2,\ldots n$$

$w(u_i, v_i)$ gives the weight for sample point (u_i, v_i) according to its magnitude of power spectrum. The measured direction is perpendicular to the lay direction of a surface. In this study, a sample size of $n = 20$ is found to be sufficient to estimate the orientation for both shaped and milled specimens. A preliminary experiment has shown that the estimation accuracy of the direction q is within 1°.

3. NEURAL NETWOROKS FOR ROUGHNESS MEASUREMENT

Once the roughness features are extracted, the second measurement task is to develop the estimation models based on the values of the selected roughness features. From

Figures 3 through 7, we found that the aforementioned features F_1 through F_5 are nonlinear functions with respect to the roughness value R_{max}. Furthermore, the values of these roughness features are affected to some extent by the specimen's orientation present to the camera. The nonlinear relationships among surface orientation, roughness features F_1 - F_5 and the corresponding roughness value R_{max} are an extremely difficult, if not impossible, task to analyze. In this study, we use artificial neural network (*ANN*) techniques to develop the estimation models for roughness measurement. The advantage of an *ANN* in measurement applications is that it provides a model-free approach for accurate estimation without knowing the exact nonlinear function between the input features and the output targets. Two neural networks are developed, one for measuring the surface roughness of machined parts in a fixed orientation, and the other one for measuring the surface roughness of machined parts in arbitrary orientations. Both neural networks used in this work are multilayer feedforward neural networks with a back-propagation learning rule (Pao 1989).

An *ANN* is specified by the topology of the network, the characteristics of the nodes and the processing algorithm. The proposed back-propagation neural networks are composed of an input layer, a single hidden layer, and an output layer. Each layer is fully connected to the succeeding layer. The outputs of nodes in one layer are transmitted to nodes in another layer through links. The link between nodes indicates flow of information during recall. During learning, information is also propagated back through the network and used to update connection weights between nodes.

Let o_j be the output of the jth node in the previous layer and w_{ij} the connection weight between the ith node in one layer and the jth node in the previous layer. The total input to the ith node of a layer is

$$net_i = \sum_j w_{ij} \cdot o_j$$

A hyperbolic tangent activation function is used here to determine the output of the node i, which is give by

$$o_i = f(net_i) = \frac{e^{net_i} - e^{-net_i}}{e^{net_i} + e^{-net_i}}$$

In the learning phase for such a network, we present the training pattern $T = \{I_p\}$, where I_p is the pth component of the vector T entered into the pth node in the input layer, and ask the network to adjust the weights in all the connecting links such that the desired outputs $\{D_k\}$ are obtained at the output nodes. Let $\{O_k\}$ be the evaluated outputs of the network in its current state. For a training pattern the squared error of the system can be written as

$$E = \frac{1}{2} \sum_k (D_k - O_k)^2$$

The generalized delta-rule learning algorithm (Rumelhart et al.1986) is applied to adjust the weights such that the error E is a minimum. A detailed derivation of the learning procedure can be found in (Pao 1989)

The first back-propagation neural network used for measuring the surface roughness of machined parts in a fixed orientation, denoted by ANN_1, is a three-layer network with one through five nodes in the input layer, depending on the number of roughness features

selected, 10 nodes in the hidden layer, and one single node in the output layer. With machined parts placed in a fixed orientation, the values of roughness features can be reliably extracted with minimum deviation. The input vector I_1 to the network is a subset of roughness features $\{ F_1, F_2, F_3, F_4, F_5 \}$. The topology of the network ANN_1 is illustrated in Figure 9. In the learning phase, the desired value of the node in the output layer is the actual roughness R_{max}^* known *a priori*. A pair of *(Input, Output)* = (I_1, R_{max}^*) forms the training sample for the network ANN_1. In the recall phase of the network, the estimated roughness R_{max} is simply given by the value of the node in the output layer.

The second back-propagation neural network, denoted by ANN_2, is used for measuring the surface roughness of machined parts in arbitrary orientations. With machined parts in arbitrary orientations, the measurement task can be carried out flexibly without the requirements of fixtures and human intervention for alignment. The topology of the network ANN_2 as shown in Figure 10 is identical to that of the network ANN_1 except that ANN_2 uses the direction feature $\boldsymbol{q}$ as the additional input. The input vector I_2 to the network ANN_2 is, therefore, contains the orientation feature $\boldsymbol{q}$ and a subset of roughness features $\{ F_1, F_2, F_3, F_4, F_5 \}$. $\boldsymbol{q}$ is used to compensate for the effect of surface orientation on the measurement error of surface roughness.

To determine an optimal subset of the five roughness features without exhaustively evaluating all possible combinations of features for both neural networks ANN_1 and ANN_2, we used the method of sequential forward selection (Nadler and Smith 1993). The

successive addition feature selection scheme proceeds as follows:

1. Select the single best feature.

2. Try all remaining features with the subset already chosen in the previous stage, one at a time, and add the one that gives the best improvement.

3. Continue the procedure above until all features are added.

In this work, the performance of a neural network with a given subset of roughness features (input vector) is measured by the root mean square (RMS) of roughness errors for a set of test data, which is defined by

$$RMS = \left[\sum_j (R^*_{max_j} - \tilde{R}_{max_j})^2 / N \right]^{1/2}$$

where $R^*_{max_j}$ is the actual roughness value, and $\tilde{R}_{max_j}$ is the estimated roughness value from the neural network for the jth sample in the test set. N is the total number of samples in the test set.

4. EXPERIMENTAL RESULTS

In this section we present experimental results for evaluating the validity of the proposed roughness features and the performance of the neural networks for roughness measurement. In our implementations, all algorithms are programmed in the C language and executed on a personal computer with a Pentium 100MHz processor. The grabbed image is of size 512x480 pixels with 256 gray levels. Standard comparison shaped

specimens (JIS B 0659) containing five roughness values of R_{max} 6.3, 12.5, 25, 50 and

100 μm, and standard comparison milled specimens containing six roughness values of

R_{max} 1.6, 3.2, 6.3, 12.5, 25 and 50 μm are used in the experiments to test the validity of

the proposed algorithms.

Illumination of the specimens is accomplished by a regular fluorescent light source

which is situated at an angle of approximately 10 degrees incidence with respect to the

normal of the specimen surface. The camera is also set up at an angle of approximately 10

degrees with respect to the normal of the specimen surface, and at a distance of

approximately 30 cm from the specimen surface. This setting enhances the characteristics of

surface patterns, and gives the best quality of surface images. Figure 11 shows the setup of

the machine vision system used in the experiments. Throughout the experiments, the camera

parameters are fixed for both shaped and milled specimens with the roughness range

between 1.6 μm and 100 μm.

For network ANN_1 that measures surface roughness of parts in a fixed orientation,

we allow the specimens to be rotated with minor angles so that precise alignment can be

eliminated. Each specimen of a given R_{max} value was rotated between -4° and 4° in

approximately 1° increments; two images of 512×480 pixels were grabbed in each

orientation. For each original image of 512×480 pixels we arbitraily selected three

distinct subimages of 256×256 pixels as the training samples for network ANN_1. The

subimage of size 256×256 pixels corresponds to approximately 4.5×4.5 mm of a

specimen surface. The sampling procedure above was also repeated, but with only one

subimage of 256×256 pixels in each grabbed image, to generate the required test samples.

For network ANN_2 that measures surface foughness of parts in arbitrary orientations, we allow the specimens to be rotated by large angles between -40° and 40° in approximately 5° increments. The sampling procedures to generate the required training set and test set for network ANN_2 are the same as those for network ANN_1, except that ANN_2 involves 17 distinct orientations and ANN_1 involves only 9 orientations for each specimen of a given roughness R_{max}. Note that none of the test samples is a redundancy of the training samples. Table 1 summarizes the number of training samples and the number of test samples used in each network for each machining.

Before we evaluate the performance of the neural networks for roughness measurement, there is an interesting feature that deserves mention here. Let $|F(0,0)|$ be the Fourier spectrum of the origin in the frequency plane, where

$$|F(0,0)| = \sqrt{P(0,0)}$$

It has been observed that the value of $|F(0,0)|$ is distributed between 25000 and 37500 for 780 training samples of shaped specimens regardless of specimen orientations, and between 40000 and 51000 for 936 training samples of milled specimens. Figure 12 shows the histogram of the Fourier spectrum $|F(0,0)|$ based on the 1716 training samples. Two well-separated distributions are resulted in the histogram, each representing a class of machining. By selecting the threshold at 39000, the feature of $|F(0,0)|$ can be used to

distinguish between shaped specimens and milled specimens. A 100% recognition rate has

been achieved for the 260 test samples of shaped specimens and 312 test samples of milled

specimens. Since the observation above is based on the shaped specimens with roughness

range between 6.3 μm and 100 μm and the milled specimens with roughness range

between 1.6 μm and 50 μm, the distribution of the Fourier spectrum $\left| F(0,0) \right|$ for

roughness values outside the specified roughness ranges may need further investigation.

The performances of networks ANN_1 and ANN_2 for shaped and milled specimens

are discussed separately in the following subsections.

4.1 Experiments on Shaped Specimens

The sequential feature selection procedure described in section 3 is applied to

determine the best combination of roughness features F_1 through F_5 in terms of minimum

RMS roughness error. The results of feature selection for networks ANN_1 (fixed

orientation) and ANN_2 (arbitrary orientation) are reported in Table 2 and Table 3,

respectively. Each entry in Table 2 and Table 3 is the RMS roughness error in μm of 90

and 170 test samples, respectively. The first row in Table 2 shows the RMS errors when

only a single roughness feature is used as the input to the network ANN_1. It indicates that

major peak frequency F_1 yields the minimum RMS error of 0.0098 μm. The second

row in Table 2 shows the results of two features that contain feature F_1 selected in the

previous stage and any one of the four remaining features. For two features selected, the

combination of features F_1 and F_5 yields the minimum RMS error of 0.0232 mm. The remaining entries in rows 3, 4 and 5 of Table 2 are interpreted in a similar way as above. From Table 2, it can be seen that adding more number of roughness features to the network may not improve the RMS error. Major peak frequency F_1 seems to dominate all other roughness features. This may be due to the fact that feature F_1 is a robust indication of feedmark spacing, and feed distance has been shown (Amstead et al. 1987) to be highly correlated with the roughness height. Therefore, for shaped specimens in a fixed orientation, major peak frequency F_1 is the best feature for measuring the surface roughness.

Table 4 presents the mean R_{max} values, maximum R_{max} values, minimum R_{max} values, and variances of R_{max} values for the test samples of shaped specimens using the network ANN_1 with feature F_1 as the input. The results reveal that the measured mean R_{max} values are almost identical to the standards. Recall that the specimens under test are allowed to be rotated within $\pm 4^o$. Network ANN_1 with input feature F_1 has shown its robustness and stability for roughness measurement with R_{max} variances less than 0.001 mm.

For shaped specimens in arbitrary orientations, Table 3 shows that major peak frequency F_1 also outperforms all other roughness features when only a single feature is used as the input to the network ANN_2. The overall minimum RMS error of 1.3177 mm is generated by the combination of three features F_1, F_5 and F_4. The improvement

in the RMS error with features F_1, F_5 and F_4 is not very significant, compared to the RMS error of 1.9474 mm with feature F_1 alone. Table 5 shows the mean R_{max} values, maximum R_{max} values, minimum R_{max} values and variances of R_{max} values for the test samples of shaped specimens using the network ANN_2 with direction feature q and roughness features F_1, F_5 and F_4 as the input. Even though the specimens under test are rotated arbitrarily within large angle range of $\pm 40^o$, the measured mean R_{max} values are also almost identical to the standards. As expected, the variance of R_{max} values generated by network ANN_2 is larger than that generated by network ANN_1 owing to arbitrary orientations of specimens present to the camera. The resulting variances of R_{max} values are generally less than 0.6mm for various roughness standards.

4.2 Experiments on Milled Specimens

Table 6 summarizes the results of the sequential feature selection procedure for milled specimens in fixed orientation ($\pm 4^o$). The first row in Table 6 also shows that major peak frequency F_1 yields the minimum RMS error of 0.0093 mm when only a single roughness feature is used as the input to the network ANN_1. From Table 6, the overall minimum is given by the combination of two features F_1 and F_5 with the RMS error of 0.0087 mm, which is not statistically different from 0.0093 mm given by single feature F_1. Table 7 presents the mean and deviation of R_{max} values for the test samples of milled specimens using the network ANN_1 with feature F_1 as the input. The results also show that the measured mean R_{max} values are almost identical to the standards, and the

variances of R_{max} values are smaller than 0.001 mm. Therefore, major peak frequency F_1 is a very effective and reliable feature for measuring the roughness of both shaped and milled surfaces in a fixed orientation.

Table 8 reports the results of the sequential feature selection procedure for milled specimens in arbitrary orientations ($\pm 40^o$). Given that only one roughness feature is used as the input to the network ANN_2, the feature of average power spectrum F_3 yields the minimum RMS error of 1.2863 mm. The overall minimum RMS error of 0.8311 mm is given by the combination of three features F_3, F_1 and F_5. Table 9 presents the mean and deviation of R_{max} values for the test samples of milled specimens using the network ANN_2 with the input vector containing the direction feature q and the roughness features F_3, F_1 and F_5. The resulting mean R_{max} values are also very close to the standards. As expected, the variance of R_{max} values generated by network ANN_2 is significantly larger than that generated by network ANN_1 due to arbitrary orientations of specimens present to the camera. For workpieces in arbitrary orientations, the R_{max} variances of milled specimens are larger than those of shaped specimens. This is due to the fact that the surface patterns of shaped specimens are more regular and have less noisy elements, compared with the surface patterns of milled specimens, as seen in Figures 1 and 2.

Based on the experimental results above, the proposed machine vision approach can be applied effectively and reliably to measure the surface roughness of interest among a set of standard surfaces of known roughness values.

5. CONCLUSION

In this paper, we have proposed a non-contact machine vision system for measuring roughness of shaped and milled surfaces. It provides a reliable assessment of surface roughness over a given 2-D area rather than a single 1-D trace. Since shaped and milled surfaces are directional patterns with the appearance of periodic, parallel feedmarks, the roughness features are extracted in the spatial frequency domain based on the 2-D Fourier transform.

The FT approach characterizes the surface image in terms of frequency components. The magnitude of frequency components enhances the periodically- occurring features present in the surface image, and the directionality of frequency components preserves the lay direction of a surface. Five roughness features have been proposed in this work. Among these features, major peak frequency F_1, which represents the frequency (or, inversely, the wavelength) of the feedmarks in the image, generally outperforms other roughness features for roughness measurement. A direction feature q has also been derived for measuring the direction of the surface present to the camera.

Two neural networks ANN_1 and ANN_2 are developed. Network ANN_1 is used for machined parts placed in a fixed orientation, and network ANN_2 is for machined parts placed in random orientations. As expected, roughness values measured by network ANN_1 are very accurate and reliable, even when the specimens under test are rotated within $\pm 4^o$. No exact alignment for test parts is required to apply network ANN_1.

Roughness values measured by network ANN_2 are also accurate but with larger deviation, compared with thosed measured by network ANN_1. Since network ANN_2 allows parts of interest to be present to the camera in arbitrary orientations, it is flexible for measurement applications without the requirements of human intervention and alignment devices.

Based on the experimental results described previously, the recommended roughness features for shaped and milled surfaces in fixed and arbitrary orientations are summarized in Table 10.

The computational time of the Fourier transform with size 256×256 is approximately 2 seconds on a Pentium 100MHz personal computer. It compares favorably with the traditional stylus-based methods. We believe the computational time can be further reduced with a high-end personal computer or workstation, or with hardware implementation of the Fourier transform for on-line, real time measurement of surface roughness.

REFERENCES

Al-kindi, G. A., Baul, R. M., and Gill, K. F., 1992, An application of machine vision in the automated inspection of engineering surface. International Journal of Production Research, 30, 241-253.

Amstead, B. H., Ostwald, P. F., and Begeman, M. L., 1987, Manufacturing Processes (John Wiley & Sons).

Chen, F. L., Joo, D , and Black, J. T. 1994, Investigation of cutting condition monitoring by visual measurement of surface texture parameters. International Journal of Computer Integrated Manufacturing, 7, 307-319.

Gonzalez, R. C., and Woods, R. E., 1992, Digital Image Proceesing (Addison-Wesley Publishing).

Hoy, D. E. P, and Yu, F., 1991, Surface quality assessment using computer vision methods. Journal of Materials Processing Teachnology, 28, 265-274.

Liu S. -S, and Jernigan, M. E., 1990, Texture analysis and discrimination in additive noise. Computer Vision, Graphics, and Image Processing, 49, 52-67.

Luk, F., and Huynh, V., 1987, A vision system for in-process surface quality assessment. Proceedings of the Vision ' 87 SME Conference, Detroit, Michigan, 12-43 to 12-58.

Nadler, M., and Smith, E. P., 1993, Pattern Recognition Engineering (John Wiley & Sons).

Pao,Y. -H., 1989, Adaptive Pattern Recognition and Neural Networks (Addison-Wesley Publishing).

Rumelhart, D. E., Hinton, G. E., and Williams, R. J., 1986, Learning internal representations by error propagation. in D. E. Rumelhart and J. L. McCelland (ed.), Parallel Distributed Processing: Explorations in the Microstructures of Cognitions: Vol. 1, Foundations, 318-362 (MIT Press).

Scott, W, and Baul, R. M.,1980, Preliminary evaluation of proximity transducer for the measurement of surface texture. International Conference on Metrology and Properties of Engineering Surfaces, Wear, 57, 33-38.
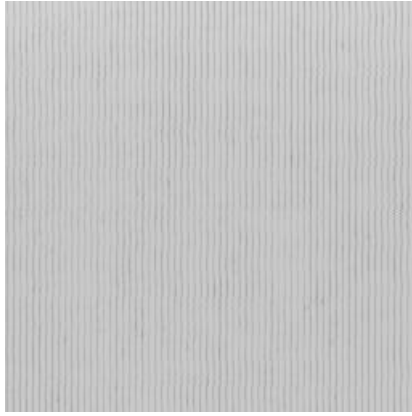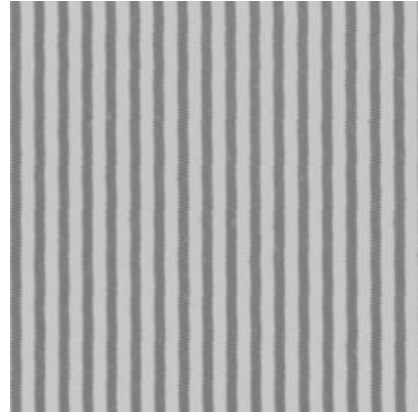
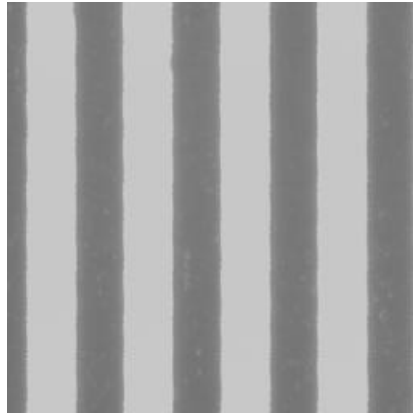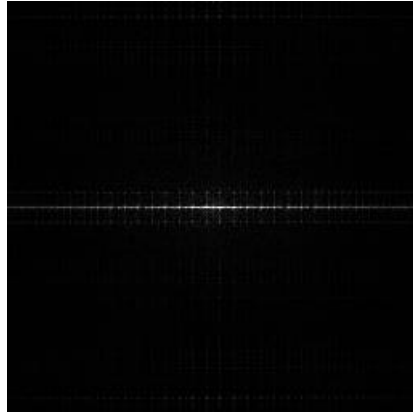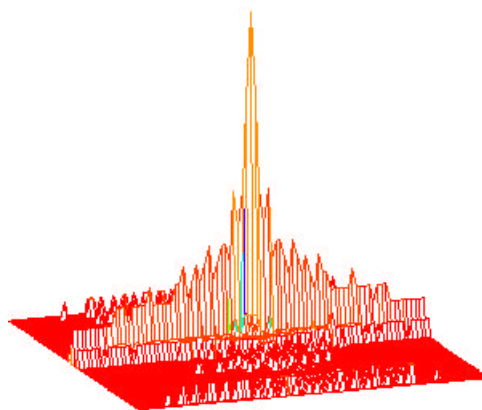(a) $R_{max} = 6.3\,\text{m}m$ (b) $R_{max} = 25\,\text{m}m$
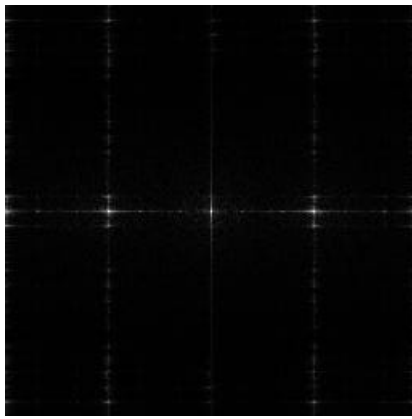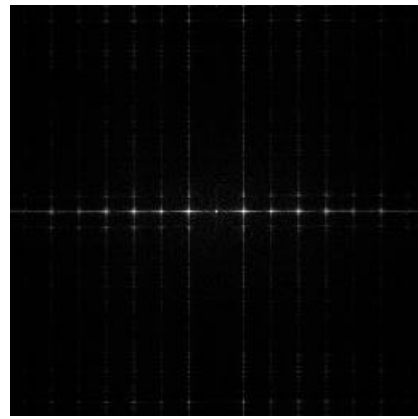
(d) (e)
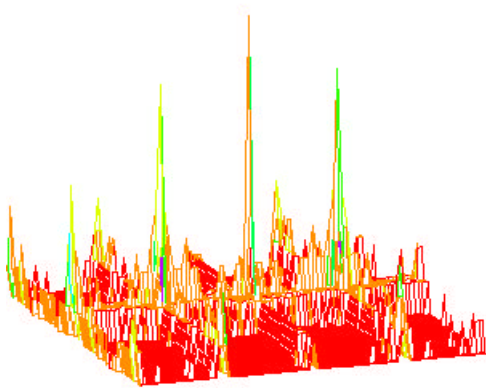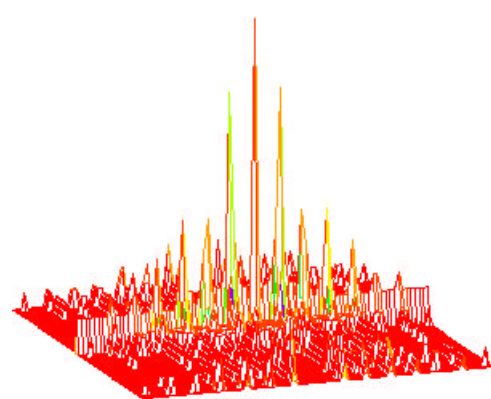
(g) (h)

Figure 1. (a), (b), (c) Surface images of shaped specimens with roughness R_{max} values of 6.3, 25 and 100 mm, respectively; (d), (e), (f) the corresponding power spectra displayed as an intensity function; and (g), (h), (i) the corresponding power spectra in 3-D perspective.
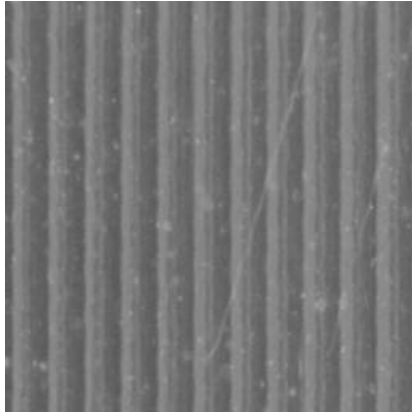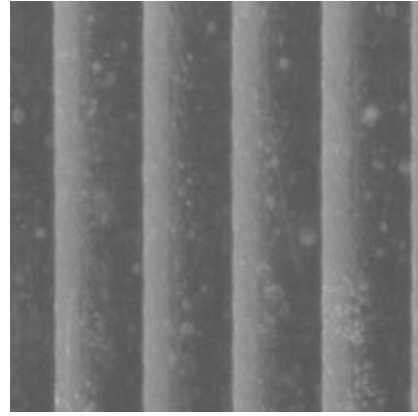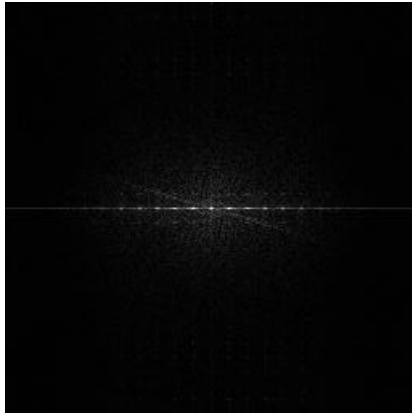
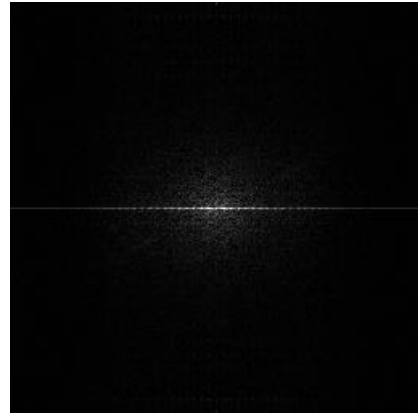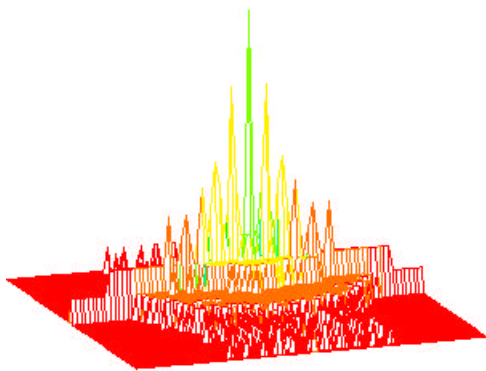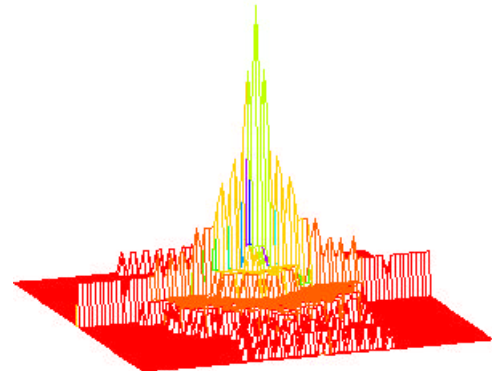(c) $R_{max} = 100\,\text{nm}$

(f)

(i)

Figure 1. (Continued)

(a) $R_{max} = 1.6\,\mu m$ (b) $R_{max} = 12.5\,\mu m$
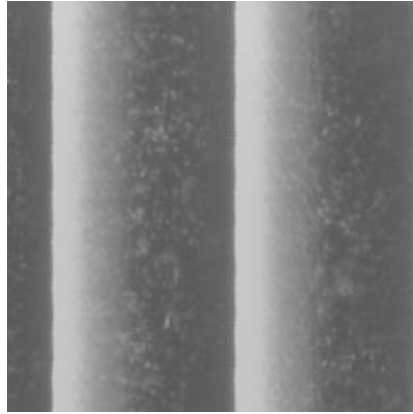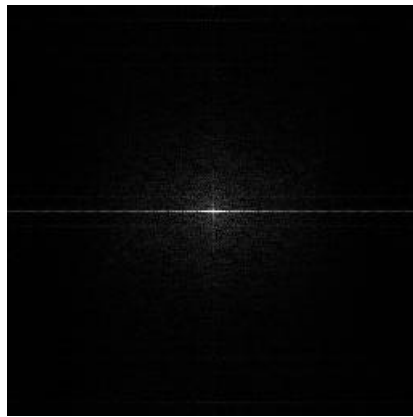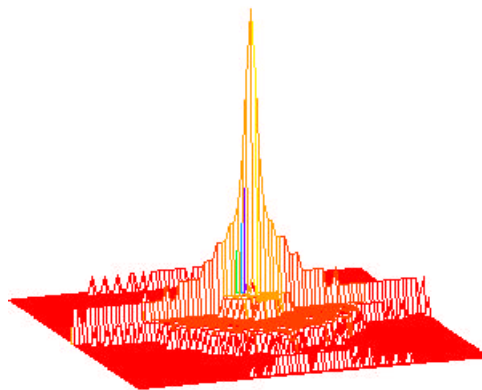
(d)   (e)

(g)   (h)

Figure 2. (a), (b), (c) Surface images of milled specimens with roughness R_{max} values of 1.6, 12.5, and 50 μm, respectively; (d), (e), (f) the corresponding power spectra displayed as an intensity; and (g), (h), (i) the corresponding power spectra in 3-D perspective.

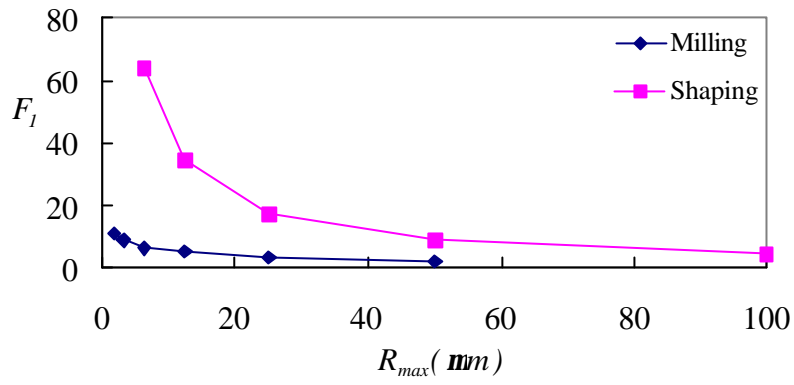(c) $R_{max} = 50\,nm$

(f)

(i)

Figure 2. (Continued)

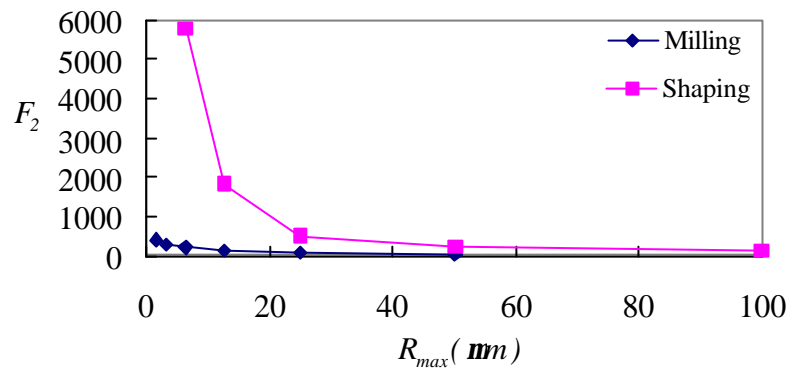Figure 3. The relationship between feature F_1 and roughness $R_{\max}$.

Figure 4. The relationship between feature F_2 and roughness $R_{\max}$.
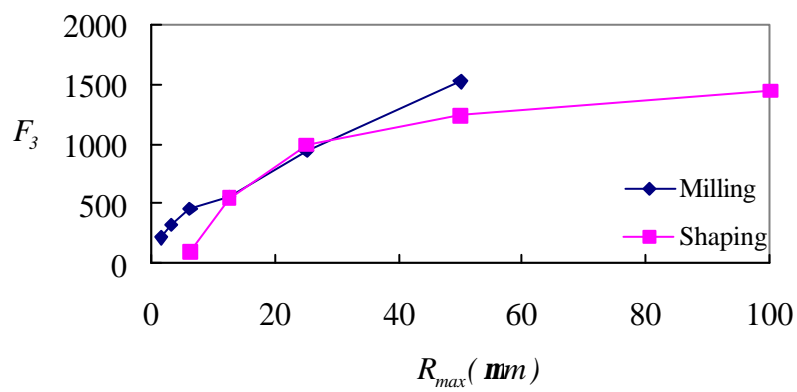

Figure 5. The relationship between feature F_3 and roughness $R_{\max}$.
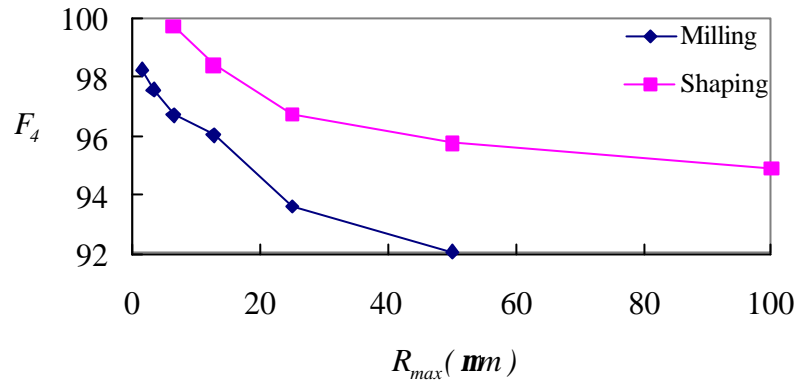
Figure 6. The relationship between feature F_4 and roughness R_{max}.

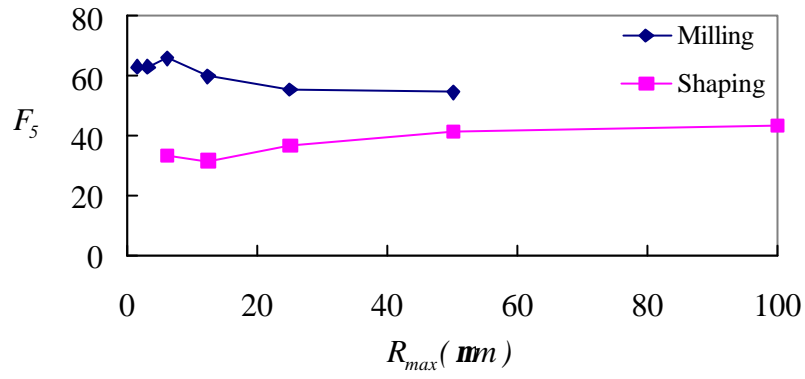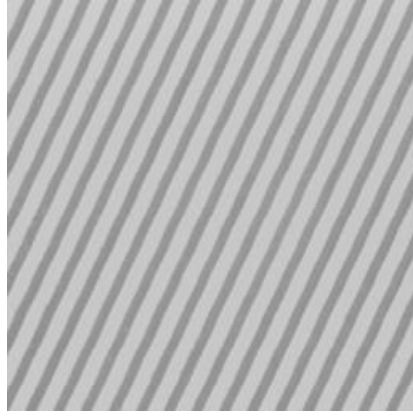Figure 7. The relationship between feature F_5 and roughness R_{max}.

(a)
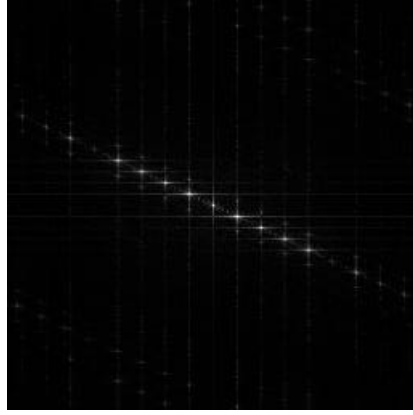
(b)

Figure 8. (a) The surface image of a shaped specimen with $R_{\max}$ 25 $\textbf{\textit{m}}$m , which is rotated by an angle 30° with respect to the original image in Figure 1(b); (b) the corresponding power spectrum displayed as an intensity function. Note that the frequency direction is perpendicular to the lay direction.

Output layer

Hidden layer

Input layer

F_i F_j
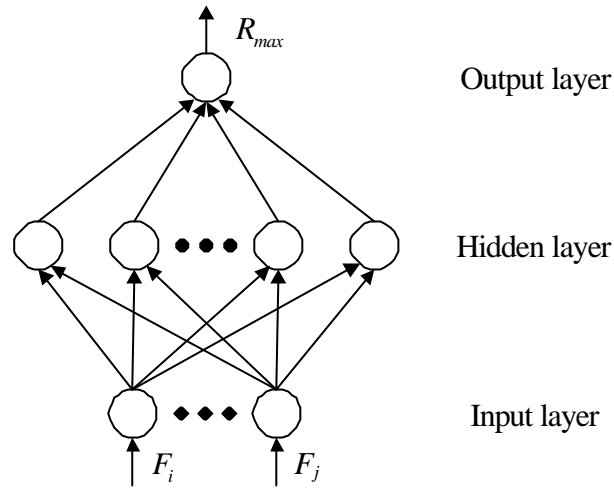
Figure 9. The system architecture of ANN_1 for workpieces in a fixed orientation.

R_{max}

Output layer

Hidden layer

Input layer

q F_i F_j

Figure 10. The system architecture of ANN_2 for workpieces in arbitrary orientations.
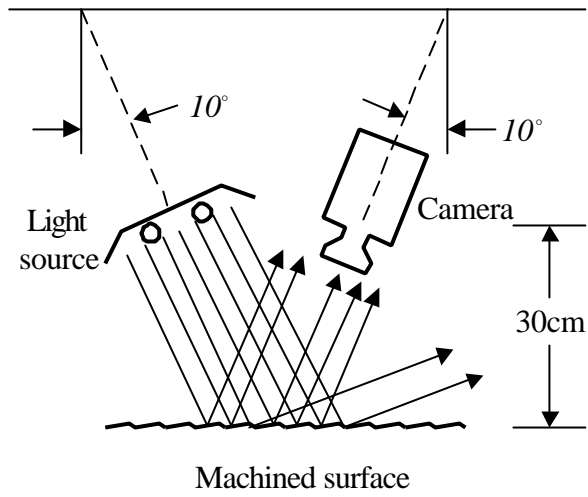
Figure 11. The machine vision setup used in the experiments.
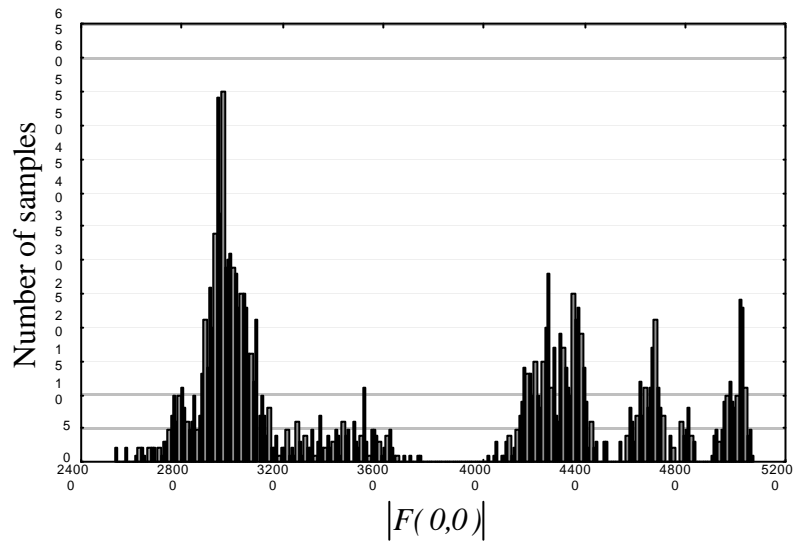
Figure 12. Distribution of the Fourier spectrum $\left|F(0,0)\right|$ for shaped and milled samples.
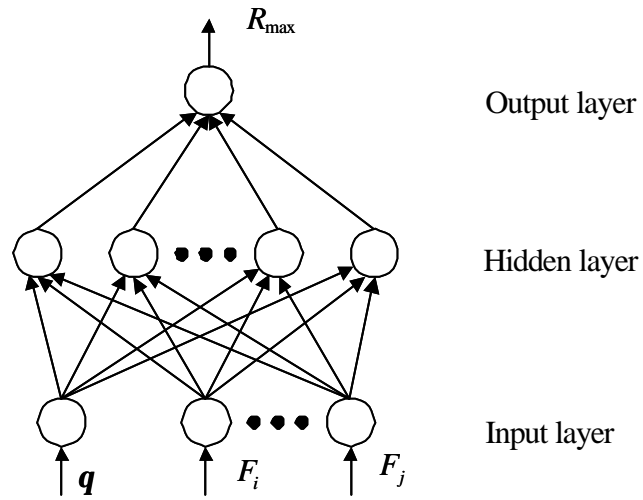
Table 1. Numbers of training samples and numbers of test samples used in the experiments.

		Network ANN$_1$ (Fixed orientation)	Network ANN$_2$ (Arbitrary orientation)
Shaping	Training samples	270	510
	Test samples	90	170
Milling	Training samples	324	612
	Test samples	108	204

Table 2. The results of feature selection for network ANN$_1$ (shaped specimens in a fixed orientation).

Feature Selection procedure	F_1	F_2	F_3	F_4	F_5	Best features selected
1 feature	0.0098	3.2241	5.9915	5.6449	25.7127	$F_1{}^*$
2 features		0.1984	0.2303	0.2404	0.0232	F_1, F_5
3 features		0.1392	0.2501	0.2152		F_1, F_5, F_2
4 features			0.2459	0.2397		F_1, F_5, F_2, F_4
5 features			0.1864			F_1, F_5, F_2, F_4, F_3

Table 3. The results of feature selection for network ANN_2 (shaped specimens in arbitrary orientations).

Feature Selection procedure	F_1	F_2	F_3	F_4	F_5	Best features selected
1 feature	1.9474	2.6683	9.8628	9.4411	21.7451	F_1
2 features		1.7561	1.6038	1.6960	1.5507	F_1, F_5
3 features		1.7943	1.3541	1.3177		F_1, F_5, F_4 *
4 features		1.4185	1.5642			F_1, F_5, F_4, F_2
5 features			1.9312			F_1, F_5, F_4, F_2, F_3

Table 4. Mean and deviation of measured R_{max} values of shaped specimens for the network ANN_1 with a single roughness feature F_1.

Shaped specimens		R_{max} (mm) standards				
		6.3s	12.5s	25s	50s	100s
F_1	Mean	6.295	12.503	25.005	50.002	100.000
	Maximum	6.297	12.515	25.029	50.002	100.000
	Minimum	6.290	12.487	24.985	50.002	100.000
	Variance	0.000	0.000	0.000	0.000	0.000

Table 5. Mean and deviation of measured R_{max} values of shaped specimens for the network ANN_2 with three roughness features F_1, F_5 and F_4.

Shapes specimens		R_{max} (mm) standards				
		6.3s	12.5s	25s	50s	100s
F_1, F_5, F_4	Mean	6.306	12.519	25.137	50.607	100.220
	Maximum	6.802	12.817	26.281	52.607	100.766
	Minimum	6.043	12.293	23.613	49.419	99.044
	Variance	0.028	0.014	0.511	0.607	0.155

Table 6. The result of feature selection for network ANN$_1$ (milled specimens in a fixed orientation).

Feature / Selection procedure	F_1	F_2	F_3	F_4	F_5	Best features selected
1 feature	0.0093	6.3541	1.5551	2.4378	14.2074	F_1
2 features		0.1142	0.0792	0.1191	0.0087	F_1, F_5 *
3 features		0.1179	0.1326	0.0954		F_1, F_5, F_4
4 features		0.2338	0.3201			F_1, F_5, F_4, F_2
5 features			0.1976			F_1, F_5, F_4, F_2, F_3

Table 7. Mean and deviation of measured R_{max} values of milled specimens for the network ANN$_1$ with a single roughness features F_1.

Milled specimens		R_{max} (mm) standards					
		1.6s	3.2s	6.3s	12.5s	25s	50s
F_1	Mean	1.600	3.203	6.300	12.500	25.000	50.000
	Maximum	1.610	3.208	6.300	12.500	25.000	50.000
	Minimum	1.573	3.168	6.300	12.500	25.000	50.000
	Variance	0.000	0.000	0.000	0.000	0.000	0.000

Table 8. The result of feature selection for network ANN$_2$ (milled specimens in arbitrary orientation).

Feature / Selection procedure	F_1	F_2	F_3	F_4	F_5	Best features selected
1 feature	1.8681	4.1019	1.2863	3.5123	15.1313	F_3
2 features	1.0492	1.1539		1.0748	1.1421	F_3, F_1
3 features		0.8866		0.8561	0.8311	F_3, F_1, F_5 *
4 features		0.9250		0.8386		F_3, F_1, F_5, F_4
5 features		0.8748				F_3, F_1, F_5, F_4, F_2

Table 9. Mean and deviation of measured R_{max} values of milled specimens for the network ANN$_2$ with three roughness features F_3, F_1 and F_5.

Milled specimens		R_{max} ($\mathbf{\mu}m$) standards					
		1.6s	3.2s	6.3s	12.5s	25s	50s
F_3, F_1, F_5	Mean	1.765	3.085	6.717	12.523	24.874	49.878
	Maximum	2.283	3.656	7.477	14.393	26.751	50.630
	Minimum	1.401	2.635	5.648	9.496	20.174	48.967
	Variance	0.053	0.068	0.222	1.259	0.856	0.152

Table 10. The recommended roughness features for measuring roughness of shaped and milled surfaces.

Machining	Orientation	Neural network	Recommended input features	Comments
Shaping	Fixed	ANN$_1$	F_1	•Accurate and reliable measurements •Limited rotated angles of surface
	Arbitrary	ANN$_2$	$\mathbf{q}, F_1, F_5, F_4$	•Good measurement with minor deviation •Flexible for measurement tasks
Milling	Fixed	ANN$_1$	F_1	•Accurate and reliable measurements •Limited rotated angles of surface
	Arbitrary	ANN$_2$	$\mathbf{q}, F_3, F_1, F_5$	•Good measurement with minor deviation •Flexible for measurement tasks